An Analytical and Numerical Analysis of Several Locally Conformal FDTD Schemes

Chris J. Railton, *Member, IEEE,* and John B. Schneider, *Member, IEEE*

***Abstract*— The virtues of the finite-difference time-domain (FDTD) method for the electromagnetic analysis of arbitrary complex metal and dielectric structures are well known. Almost equally well known are the difficulties encountered by the technique when the material boundaries do not coincide with the Cartesian mesh. Until recently, there were few alternatives to the simple, but inaccurate, staircase approximation for these cases. However, over the past few years, there have been several solutions proposed, which maintain the simplicity and efficiency of the FDTD method while providing an accurate treatment of curved, offset, or sloping metallic boundaries. In this paper, analytical and numerical comparisons are presented and a clear recommended method is shown to emerge.**

***Index Terms*— FDTD methods.**

I. Introduction

WHILE THE finite-difference time-domain (FDTD) method continues to enjoy ever-increasing popularity due to its simplicity, efficiency, and generality, the problem of modeling geometries which contain material boundaries that do not coincide with the Cartesian axes remains to be definitively resolved. Over the past years, a number of techniques have been proposed to deal with this difficulty and, recently, several interesting approaches have appeared in the literature. It is the purpose of this paper to examine, both from an analytical and a numerical perspective, the most promising of these and to establish the method of choice for the FDTD practitioner.

The simplest, earliest, and arguably still the most frequently used way of addressing the problem of curved surfaces is by means of a staircase approximation. Although trivially simple, this method is known to introduce errors which persist even when the mesh size is made very small [1]–[3]. In order to improve upon this without going into the complexity of generalized nonorthogonal coordinates or totally unstructured grids, the FDTD algorithm was reformulated in terms of surface and contour integrals. This facilitated the incorporation of curved perfectly electrically conducting (PEC) boundaries [4] and was applied to various scattering problems such as radar cross section (RCS) calculations for double spheres [5]. While this method, dubbed the contour-path FDTD (CP-FDTD) method, is clearly successful for a variety of scattering problems, it has been shown that, due to the noncausal and nonreciprocal nearest neighbor approximation which is invoked, the technique is likely to exhibit late time instability regardless of how small a time step is used [6]–[8]. This is especially true for the case of resonant structures where there is no mechanism for the dissipation of spuriously generated energy.

In 1995, two different methods were published by which general three-dimensional (3-D) PEC structures could be analyzed using a modified form of the CP-FDTD method, which restored the reciprocity of the algorithm. In [9] and [10], hereafter referred to as the A-FDTD method, the problem of overcoming the difficulties associated with the nearest neighbor borrowing is solved by multiplying the borrowed field by a factor of between zero and unity. Reciprocity is established if this factor is zero and stability is assured only under this condition. At about the same time, in [11] and [12], a different approach was proposed, hereafter referred to as the stabilized CP-FDTD method, which restored reciprocity by means of adding a term to the update equations for the E fields. Both these methods have been shown to give accurate results and to be late-time stable for a suitably chosen time step.

More recently, a scheme was published [13], [14], which is also reciprocal and has been shown to provide accurate results and, in addition, is much simpler than the approaches described in [10] and [12]. In this technique, hereafter referred to as the D-FDTD method, the distorted cells are always contracted, never expanded, and the E-field update equations are left unmodified. In this paper, it will be shown that this method, despite its simplicity, decisively outperforms the others. The only penalty is the need to use a time step which is 50%–70% of that allowable in the unmodified algorithm. It is considered that this cost is small compared to the benefits of using the method.

A version of the CP-FDTD method has been published [15] in which the volume form of Ampere's and Faraday's laws are employed. This method may be expected to provide improved accuracy over the traditional CP-FDTD, but it shares the property of nonreciprocal nearest neighbor borrowing and potential late-time instability.

It is noted that none of these methods can be directly applied to dielectric boundaries. Although a two-dimensional (2-D) example of the use of a CP-FDTD method for dielectric boundaries has been published [4], the extra difficulties which arise when the tangential electric field on the boundary is nonzero are such that the method is impracticable. In those

Manuscript received January 9, 1998; revised September 2, 1998. This work was supported by the Office of Naval Research, Code 321OA.

C. J. Railton is with the Centre for Communications Research, Faculty of Engineering, University of Bristol, Bristol BS8 1TR, U.K.

J. B. Schneider is with the School of Electrical Engineering and Computer Science, Washington State University, Pullman, WA 99164-2752 USA (e-mail: schneidj@eecs.wsu.edu).

Publisher Item Identifier S 0018-9480(99)00385-3.

cases, either a simple improvement on the staircase [16] or the more complex, but more accurate, locally [17] or globally nonorthogonal grids may be used. In addition to these methods which apply to general 3-D FDTD analyses, a conformal method was proposed in 1985 [18], which was applied to planar circuit analysis. More recently, a conformal method for 3-D problems, based on the transmission-line matrix (TLM) method was also published [19].

II. Reflection Coefficients for Offset Planes

Here, we consider the reflection coefficients that are obtained from the CP-FDTD and D-FDTD methods for planar boundaries that are aligned with, but offset from, the nodes in the grid. These reflection coefficients can be obtained analytically and are thus compared to the exact reflection coefficients. It is shown that the CP-FDTD and D-FDTD reflection coefficients are identical to each other for "contracted" cells, but they differ when the boundary is such that an "extended" cell is used in the CP-FDTD method. In situations where the coefficients differ, the D-FDTD method typically yields the more accurate result. To illustrate the analysis, we present the derivation for the one-dimensional (1-D) case. The reflection coefficients for the 2-D TE and TM cases are also presented. However, since the 2-D derivations are straightforward, but lengthy, only the major steps in the derivation are described.

A. 1-D Reflection Coefficients

Consider a 1-D space where a y-polarized harmonic plane traveling in the $+x$-direction is incident upon a PEC boundary at $x = b$. The total field is given by

$$E_y(x,t) = (e^{-jkx} + Re^{jkx})e^{j\omega t} \tag{1}$$

where k is the free-space wavenumber, ω is the frequency, and R is the reflection coefficient. Setting $E_y(x)$ to zero at $x = b$ and solving for the reflection coefficient yields

$$R = -e^{-j2kb}. \tag{2}$$

In an FDTD simulation, the incident electric and magnetic fields are given by

$$E_y^{\text{inc}}(x,t) = e^{j(\omega t - \tilde{k}x)} \tag{3}$$

$$H_z^{\text{inc}}(x,t) = \frac{1}{\tilde{Z}} e^{j(\omega t - \tilde{k}x)} \tag{4}$$

where $\tilde{k}$ is the numeric wavenumber, $\tilde{Z}$ is the numeric characteristic impedance, and x and t are sampled at discrete points in space and time, respectively. Using these fields in the standard second-order Yee FDTD algorithm, it is easy to relate the numeric impedance to the free-space impedance Z, e.g., [20, Sec. 5.3]. The result is

$$\tilde{Z} = \frac{Z \sin(\omega \delta t/2)}{S \sin(\tilde{k}\Delta x/2)} \tag{5}$$

where $S = c\delta t/\delta x$ is the Courant number. (Employing the 1-D dispersion relation, the expression on the right reduces to Z, i.e., $\tilde{Z} = Z$ in 1-D problems. However, for simplification of subsequent results, it is convenient to leave the numeric impedance, as given by (5). Also, in higher dimensions, the numeric and continuous-world impedances differ, thus we maintain the distinction here.) When the field is incident on a PEC, the total field to the left of the boundary is given by

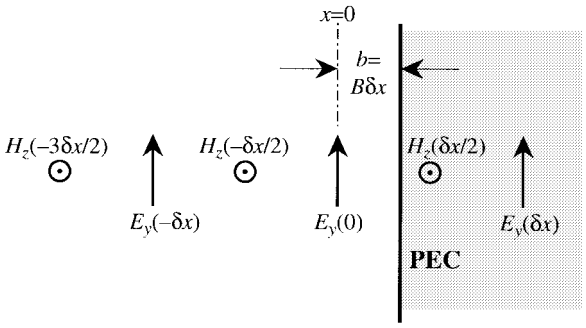

Fig. 1. 1-D computational domain. In the D-FDTD method, for all offsets such that $1/15 < B \leq 1$, only the node $H_z(\Delta x/2)$ uses a modified update equation. In the CP-FDTD method, for offsets $0 \leq B < 1/2$, the node $E_y(0)$ is unused and the node $H_z(-\delta x/2)$ uses a modified update equation. This results in an extended cell. For offsets $1/2 \leq B \leq 1$, the CP-FDTD method is the same as the D-FDTD method, i.e., $H_z(\delta x/2)$ is the last node in the grid and it employs a contracted cell.

$$E_y(x,t) = (e^{-j\tilde{k}x} + \tilde{R}e^{j\tilde{k}x})e^{j\omega t} \tag{6}$$

$$H_z(x,t) = \frac{1}{\tilde{Z}}(e^{-j\tilde{k}x} - \tilde{R}e^{j\tilde{k}x})e^{j\omega t} \tag{7}$$

where $\tilde{R}$ is the numeric or FDTD reflection coefficient.

To derive the reflection coefficient for the D-FDTD method, assume, without loss of generality, that, as shown in Fig. 1, an E_y node is located at $x = 0$ and the PEC boundary is offset a distance b to the right of this node ($0 \leq b \leq \delta x$). In the D-FDTD method, the update equation for the H_z node located at $x = \delta x/2$ is given by

$$H_z\left(\frac{\delta x}{2}, \left[n+\frac{1}{2}\right]\delta t\right) = H_z\left(\frac{\delta x}{2}, \left[n-\frac{1}{2}\right]\delta t\right) + \frac{\delta t}{\mu b} E_y(0, n\delta t). \tag{8}$$

All other nodes to the left of the boundary are updated in the usual way. Note that (8) is applied to the H_z node at $\delta x/2$ even when this node is beyond the PEC boundary. However, before (8) is applied, b must meet certain restrictions, which will be considered below. The location of the PEC enters into this equation through b in the denominator of the coefficient of $E_y(0, n\delta t)$. By substituting (6) and (7) into (8) and solving for the reflection coefficient, the following is obtained:

$$\tilde{R} = -\frac{\tilde{Z}\frac{\delta t}{\mu b} - j2\sin(\omega\delta t/2)e^{-j\tilde{k}\delta x/2}}{\tilde{Z}\frac{\delta t}{\mu b} + j2\sin(\omega\delta t/2)e^{j\tilde{k}\delta x/2}}. \tag{9}$$

Equation (9) can be simplified by using (5) and Euler's formula to expand the complex exponentials. Defining the normalized offset B by $B = b/\delta x$, the resulting expression for the reflection coefficient is

$$\tilde{R} = -\frac{B[e^{-j\tilde{k}\delta x} - 1] + 1}{B[e^{j\tilde{k}\delta x} - 1] + 1}. \tag{10}$$

Comparing (10) to the exact expression in (2), we note that both are equal to -1 when the offset b (and, hence, B)

is zero. When the offset is the width of the entire cell, i.e., $b = \delta x$ ($B = 1$), the exact reflection coefficient is $R = -\exp(-j2k\delta x)$, while the D-FDTD method yields $\tilde{R} = -\exp(-j2\tilde{k}\delta x)$. If the difference between the numeric wavenumber and the continuous one is ignored, these results are identical. Another way (10) and (2) can be compared is by expanding the exponentials in (10) in Taylor series and retaining only the first two terms. This yields

$$\tilde{R} \approx -\frac{1 - j\tilde{k}B\delta x}{1 + j\tilde{k}B\delta x}. \tag{11}$$

The right-hand side is that which is obtained from the Taylor series expansion of $\exp(-j\tilde{k}B\delta x)$ over the expansion of $\exp(j\tilde{k}B\delta x)$. The ratio of the these two complex exponentials is $\exp(-j2\tilde{k}B\delta x)$ which is the same as (2), except the numeric wavenumber is used.

The dispersion relation for the Yee algorithm is well known [20], [21] and has a simple closed-form representation in one dimension. It is found most convenient to write the dispersion relation is terms of the number of points-per-wavelength N_λ and the Courant number S. The result is

$$\frac{1}{S}\sin\left(\frac{\pi}{N_\lambda}S\right) = \sin\left(\frac{\pi}{N_\lambda}\frac{\lambda}{\tilde{\lambda}}\right) \tag{12}$$

where λ is the free-space wavelength and $\tilde{\lambda}$ is the numeric wavelength. Using (12), the ratio $\lambda/\tilde{\lambda}$ can be expressed completely in terms of the point-per-wavelength and the Courant number. Now, recognizing that $\tilde{k}\delta x = (2\pi/N_\lambda)(\lambda/\tilde{\lambda})$, (12) can be combined with (10) to obtain the reflection coefficient as a function of the N_λ, S, and B, to wit

$$\tilde{R}(B, N_\lambda, S) = -\frac{B\left[e^{-jP_1(N_\lambda,S)} - 1\right] + 1}{B\left[e^{jP_1(N_\lambda,S)} - 1\right] + 1} \tag{13}$$

where

$$P_1(N_\lambda, S) = \tilde{k}\delta x = 2\sin^{-1}\left(\frac{\sin\left(\frac{\pi}{N_\lambda}S\right)}{S}\right). \tag{14}$$

Although this derivation has been presented in terms of one dimension, this expression holds in two and three dimensions—the only restriction is that the plane wave is normally incident on a planar boundary that is aligned with, but may be offset from, the nodes in the grid.

The D-FDTD method was presented as a 3-D algorithm and placed restrictions on b for (8) to hold [13], [14]. These restrictions were stated in terms of the geometry of a cell. Assuming the Courant number is half the Courant limit, these restrictions are: 1) the area outside of the PEC for a partially filled cell must be greater than 1.5% of the undistorted cell and 2) the ratio of the maximum length of a segment outside the PEC to the area outside the PEC must be less than 15. Note that the second restriction was stated as a ratio of a length to an area. For square cells (i.e., $\delta x = \delta y$), this restriction can be meaningfully interpreted. However, for cells with unequal sides, no clear interpretation of the second restriction has been put forward. Nevertheless, these restrictions can be applied to the 1-D analysis by associating a square cell with the nodes shown in Fig. 1. Thus, there would be E_x nodes centered above and below the H_z nodes. If this is the case, the second restriction states that b must be greater than $\delta x/15$ for (8) to hold. (The first restriction is the less restrictive of the two for the offset-plane case and, hence, does not further constrain b. For tilted boundaries, the first restriction can be the more restrictive of the two.) When b is less than $\delta x/15$, the cell can be treated as if it were completely filled with PEC. Thus, taking this restriction into account, the reflection coefficient for the D-FDTD method can be written as

$$\tilde{R}_D(B, N_\lambda, S) = \begin{cases} -1, & \text{for } 0 \le B \le 1/15 \\ \tilde{R}(B, N_\lambda, S), & \text{for } 1/15 < B \le 1 \end{cases} \tag{15}$$

where a subscript D indicates this is for the D-FDTD method. Note that instead of filling with PEC those cells that do not meet the geometry restrictions, these cells can instead be modeled with the CP-FDTD method [14]. Such a hybrid approach permits a conformal scheme to be used throughout the range of all possible offsets. The consequences of handling "small" cells by either filling with PEC or by using the CP-FDTD method will be considered below.

Before considering oblique incidence, we derive the reflection coefficient for the CP-FDTD method. In the CP-FDTD method, two types of cells are possible. The first is an "extended" cell, which occurs when the node just prior to the PEC boundary is an electric-field node. Although this electric-field node is outside the metal, it is left unused. The magnetic-field node that is outside the PEC and nearest the boundary is the last one for which an update equation is used. The cell associated with this magnetic field is "extended" due to the unused electric field adjacent to the boundary. Extended cells are obtained when $0 \le b < \delta x/2$. The second type of cell is a contracted cell, which occurs when the node just prior to the boundary is a magnetic-field node. Contracted cells are obtained when $\delta x/2 \le b \le \delta x$.

First we obtain the reflection coefficient for extended cells. In this case, the last node in the grid for which an update equation is applied is the H_z node at $-\delta x/2$. The CP-FDTD algorithm dictates that this node be updated by

$$H_z\left(-\frac{\delta x}{2}, \left[n + \frac{1}{2}\right]\delta t\right) = H_z\left(-\frac{\delta x}{2}, \left[n - \frac{1}{2}\right]\delta t\right) + \frac{\delta t}{\mu(\delta x + b)}E_y(-\delta x, n\delta t). \tag{16}$$

This equation differs from (8) in two respects: each node is shifted one grid space to the left and the geometric factor specifying the boundary location is now $\delta x + b$ (as opposed to just b). As before, one can use the field expressions (6) and (7) in (16) and solve for the reflection coefficient. Since (16) is only slightly different from (8), it is easy to express the CP-FDTD reflection coefficient in terms of the numeric reflection coefficient given in (13). The result is

$$\tilde{R}_{\mathrm{CP}}(B, N_\lambda, S) = e^{j2P_1(N_\lambda,S)}\tilde{R}(B+1, N_\lambda, S), \qquad 0 \le B < 1/2 \tag{17}$$

where the subscript CP indicates the reflection coefficient for the CP-FDTD method. As before, when the offset is zero (i.e.,

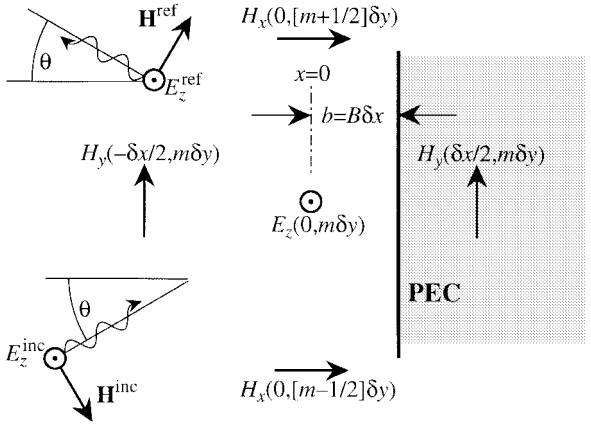

Fig. 2. 2-D computational domain for TM_z polarization. In the D-FDTD method, for all offsets such that $1/15 < B \leq 1$, only the node $H_y(\delta x/2, m\delta y)$ uses a modified update equation. In the CP-FDTD method, for offsets $0 \leq B < 1/2$, the node $E_z(0, m\delta y)$ is unused and the node $H_z(-\Delta x/2, m\delta y)$ uses a modified update equation. For offsets $1/2 \leq B \leq 1$, the CP-FDTD method is the same as the D-FDTD method.

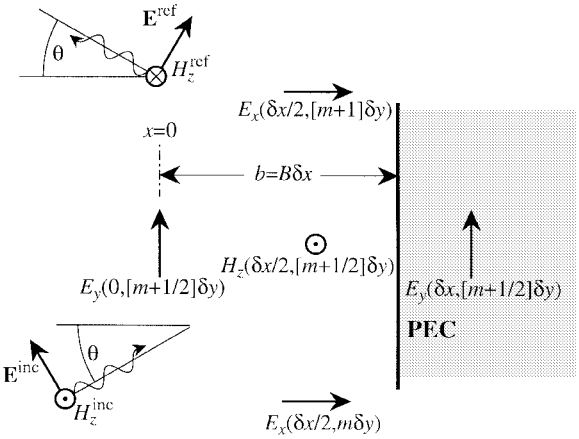

Fig. 3. 2-D computational domain for TE_z polarization. In the D-FDTD method, for all offsets such that $1/15 < B \leq 1$, only the node $H_z(\delta x/2, [m+1/2]\delta y)$ uses a modified update equation. In the CP-FDTD method, for offsets $0 \leq B < 1/2$, the node $E_y(0, [m+1/2]\delta y)$ is unused and the node $H_z(-\Delta x/2, [m+1/2]\delta y)$, which is not shown, uses a modified update equation. For offsets $1/2 \leq B \leq 1$, the CP-FDTD method is the same as the D-FDTD method.

$b = B = 0$) the result is exact since the phase of the complex exponential cancels the phase of $\tilde{R}(1, N_\lambda, S)$.

For contracted cells, the update equation, and, hence, the reflection coefficient of the CP-FDTD method is identical to that of the D-FDTD method. Thus,

$$\tilde{R}_{\mathrm{CP}}(B, N_\lambda, S) = \tilde{R}(B, N_\lambda, S) \quad 1/2 \leq B \leq 1. \tag{18}$$

B. 2-D Reflection Coefficients

Consider, as depicted in Fig. 2, TM_z harmonic illumination of a PEC plane located at $x = b$. The total fields in the FDTD grid are given by

$$E_z(x, y, t) = E_0(e^{-j\tilde{k}_x x} + \tilde{R}e^{j\tilde{k}_x x})e^{j(\omega t - \tilde{k}_y y)} \tag{19}$$

$$H_x(x, y, t) = H_{0x}(e^{-j\tilde{k}_x x} + \tilde{R}e^{j\tilde{k}_x x})e^{j(\omega t - \tilde{k}_y y)} \tag{20}$$

$$H_y(x, y, t) = H_{0y}(e^{-j\tilde{k}_x x} - \tilde{R}e^{j\tilde{k}_x x})e^{j(\omega t - \tilde{k}_y y)} \tag{21}$$

where $\tilde{k}_x = \tilde{k}\cos\theta$ and $\tilde{k}_y = \tilde{k}\sin\theta$ are the x and y components of the numeric wave vector, respectively, E_0 is an arbitrary amplitude, and θ is the incident angle. The characteristic impedance [20] of the grid dictates that the field amplitudes are related by

$$\frac{H_{0x}}{E_0} = \frac{\delta t}{\mu \delta y}\frac{\sin(\tilde{k}_y \delta y/2)}{\sin(\omega \delta t/2)} \tag{22}$$

$$\frac{H_{0y}}{E_0} = -\frac{\delta t}{\mu \delta x}\frac{\sin(\tilde{k}_x \delta x/2)}{\sin(\omega \delta t/2)}. \tag{23}$$

The 2-D dispersion relation [20] relates the components of the wave vector and the frequency via

$$\sin^2(\omega \delta t/2) = \frac{c^2 \delta t^2}{\delta x^2}\sin^2(\tilde{k}_x \delta x/2) + \frac{c^2 \delta t^2}{\delta y^2}\sin^2(\tilde{k}_y \delta y/2). \tag{24}$$

Referring to Fig. 2 and ignoring for the moment the geometry restrictions inherent in the D-FDTD method, the only nodes in the D-FDTD method that have their update equations modified by the presence of the plane are the H_y nodes located at $(\delta x/2, m\delta y)$. The update equation for these nodes is

$$H_y\left(\frac{\delta x}{2}, m\delta y, \left[n + \frac{1}{2}\right]\delta t\right) = H_y\left(\frac{\delta x}{2}, m\delta y, \left[n - \frac{1}{2}\right]\delta t\right) - \frac{\delta t}{\mu b}E_z(0, m\delta y, n\delta t). \tag{25}$$

The reflection coefficient can be obtained by plugging the field expressions (19)–(21) into (25). After considerable algebraic manipulation, and employing (22)–(24) to simplify the result, the reflection coefficient is found to be

$$\tilde{R}(B, N_\lambda, S, \theta, \alpha) = -\frac{B\left[e^{-jP_2} - 1\right] + 1}{B\left[e^{jP_2} - 1\right] + 1} \tag{26}$$

where $P_2 = \tilde{k}_x \delta x$ is, from the dispersion relation (24), a solution to

$$\sin^2\left(\frac{\pi}{N_\lambda}S\right) = S^2\sin^2\left(\frac{P_2}{2}\right) + S^2\alpha^2\sin^2\left(\frac{P_2\alpha}{2}\tan\theta\right) \tag{27}$$

where θ is the incident angle, α is the cell aspect ratio defined by $\alpha = \delta x/\delta y$, and, as before, B is the normalized offset. The spatial step in the x-direction is taken as the reference length so that $N_\lambda = \lambda/\delta x$ and $S = c\delta t/\delta x$. Note that (26) is similar to the 1-D reflection coefficient—the only difference is that $\tilde{k}$ in (10) is replaced by $\tilde{k}_x$. Thus, (10) can be considered a special case of (26) with θ equal to zero.

For TE_z polarization, a similar approach can be used to obtain the reflection coefficient. After a significant amount of algebra, the result is identical to (26). The assumed orientation of the fields and the location of the nodes necessary for (26) to pertain to the TE_z case is shown in Fig. 3.

The reflection coefficient for the D-FDTD method can now be written in terms of $\tilde{R}$, where one must account for the geometric restrictions mentioned previously. The result is

$$\tilde{R}_D(B, N_\lambda, S, \theta, \alpha) = \begin{cases} -1, & \text{for } 0 \le B \le 1/15 \\ \tilde{R}(B, N_\lambda, S, \theta, \alpha), & \text{for } 1/15 < B \le 1. \end{cases} \tag{28}$$

As was the case in one dimension, the CP-FDTD method in two dimensions yields either contracted or extended cells. When the cells are contracted, the reflection coefficients are the same as for the D-FDTD method. For extended cells, the CP-FDTD reflection coefficient can be expressed in terms of the reflection coefficient $\tilde{R}$. Thus, the reflection coefficient for the CP-FDTD method is

$$\tilde{R}_{\mathrm{CP}}(B, N_\lambda, S, \theta, \alpha) = \begin{cases} e^{j2P_2}\tilde{R}(B+1, N_\lambda, S, \theta, \alpha), & \text{for } 0 \le B < 1/2 \\ \tilde{R}(B, N_\lambda, S, \theta, \alpha), & \text{for } 1/2 \le B \le 1 \end{cases} \tag{29}$$

where P_2 is a solution to (27).

The exact reflection coefficient for 2-D is given by (2) with k replaced by $k_x = k\cos\theta$, i.e., $R = -\exp(-j2k_xB\delta x)$. However, to isolate geometric errors introduced by the conformal scheme from the inherent phase error associated with the numeric wavenumber, it is helpful to define a "numerically exact" reflection coefficient. This is the same as the exact reflection coefficient, except the continuous-world wavenumber is replaced by the numeric one, i.e.,

$$R_{\mathrm{NE}} = -e^{-j2\tilde{k}_xB\delta x}. \tag{30}$$

The magnitude of the numeric reflection coefficients is unity (the numerator and denominator are complex conjugates). Thus, neither the CP-FDTD method nor the D-FDTD method introduce any artificial dissipation for offset planes. However, the phases of the numeric reflection coefficients do differ from that of the exact value. In the direction of propagation of a harmonic plane wave, the phase associated with a spatial step is $2\pi/N_\lambda$ rad. The error is defined as the phase difference between the numerically exact and numeric reflection coefficients normalized by the per-cell phase. Thus, the error in the D-FDTD method is given by

$$\mathrm{Error} = \frac{N_\lambda}{2\pi}(\arg(R_{\mathrm{NE}}) - \arg(\tilde{R}_D)). \tag{31}$$

The error for the CP-FDTD is obtained by replacing $\tilde{R}_D$ with $\tilde{R}_{\mathrm{CP}}$ in (31).

Fig. 4 shows the error in the phase of the D-FDTD and CP-FDTD reflections for a plane wave normally incident ($\theta = 0$) on an offset plane as a function of the normalized offset B. The offset varies from zero to the entire width of the cell, while N_λ is held fixed at eight points per wavelength. The Courant number used for the CP-FDTD method is $1/\sqrt{3}$, i.e., the 3-D stability limit. The D-FDTD method requires a reduction in the Courant number in order to ensure a stable result. The worst-case reduction, according to [13] and [14], is a factor of 0.5, which is used here (using this Courant number provides the greatest geometric flexibility). However, since the wavenumber corresponding to the given Courant number is used in the numerically exact solution, the Courant number has essentially no impact on these plots. From Fig. 4, it is clear that the D-FDTD method is superior when $1/15 < B < 1/2$. When the offset is more than a half-cell, the reflection coefficients are identical. (If the true wavenumber had been used in the exact solution, the D-FDTD method would have had slightly more error than the CP-FDTD method owing to the lower Courant number.) Note that both reflection coefficients have discontinuities.

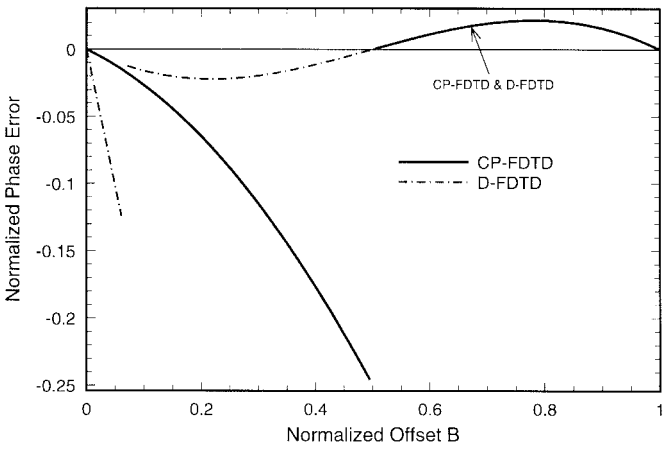

Fig. 4. Normalized phase error versus normalized offset B for normal incidence. The Courant number is $1/\sqrt{3}$ for the CP-FDTD method and $0.5/\sqrt{3}$ for the D-FDTD method. The points per wavelength N_λ is eight.

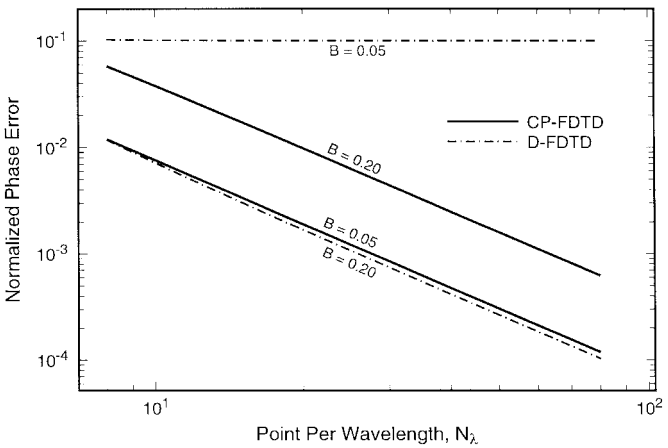

Fig. 5. Normalized phase error versus points per wavelength N_λ. The Courant numbers are the same as for the previous figure and the offset is either $B = 0.05$ or $B = 0.20$.

Fig. 5 is a log–log plot of the absolute value of the error as a function of the number of points per wavelength N_λ. The normalized offset is held fixed at either 0.05 or 0.20, while N_λ varies over one order of magnitude ($8 \le N_\lambda \le 80$). For $B = 0.20$, clearly the error, as defined by (31), is second order for both methods since the error decreases two orders of magnitude with a change of one order of magnitude in the discretization. In fact, provided that $B \ge 1/15$, this behavior is independent of the offset, i.e., for different offsets, the magnitude of the curves in Fig. 5 will change, but not the slopes. For $B = 0.05$, we have assumed the D-FDTD method

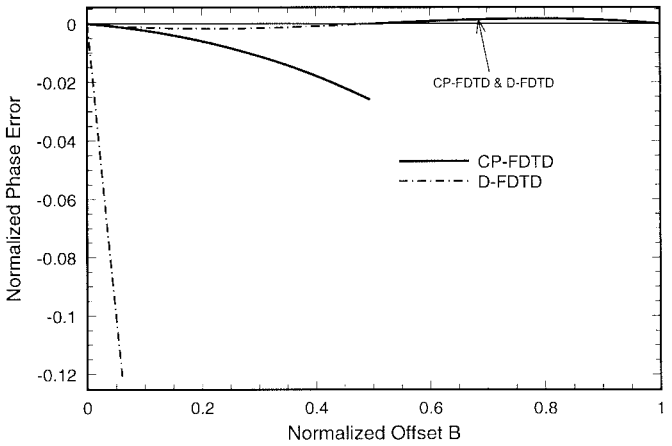

Fig. 6. Normalized phase error versus normalized offset B for normal incidence. Courant numbers are as before. $N_\lambda = 27$.

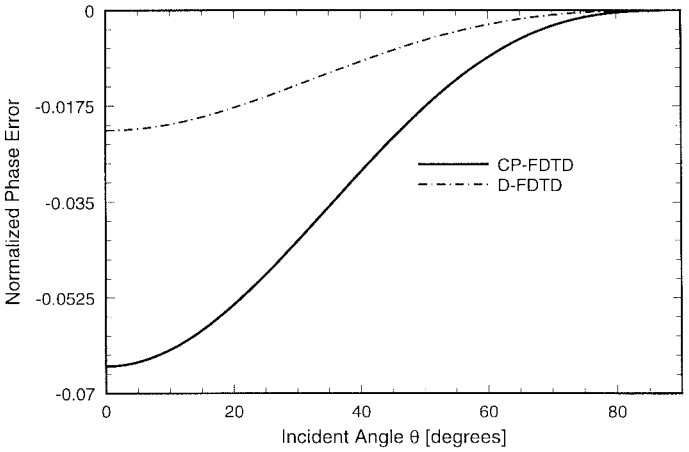

Fig. 7. Normalized phase error versus incident angle θ. The Courant numbers are the same as for the previous figures, the offset is $B = 0.2$, and the points per wavelength are $N_\lambda = 8$.

uses the staircase approximation which, on a phase normalized basis, is zeroth-order accurate. A similar flat (zeroth-order) curve pertains to the D-FDTD method for all offset such that $B < 1/15$. On the other hand, for an offset in the range $B < 1/15$ the CP-FDTD is still second-order accurate.

Given that there is a range of offsets over which the D-FDTD method employs a zeroth-order scheme and in this range the CP-FDTD method employs a second-order technique, there is a discretization beyond which the integrated error (i.e., the error over all offsets) in the CP-FDTD method is less than in the D-FDTD method. This "cross over point" occurs for an N_λ of approximately 27. Fig. 6 shows the error as a function of the normalized offset for $N_\lambda = 27$ (i.e., when the two method have approximately the same total error). However, if one employs the CP-FDTD method within the D-FDTD method to handle cells that violate the geometry restrictions, the D-FDTD reflection coefficient would no longer exhibit any zeroth-order behavior. In this case, the integrated error in the D-FDTD would be lower than the CP-FDTD method for all discretizations. In this hybrid scheme, the error in the D-FDTD method would be identical to that of the CP-FDTD scheme for $B \leq 1/15$ and then, for greater values of B, track the D-FDTD curves as shown. Note that the discontinuity associated with switching from the CP-FDTD scheme to the D-FDTD scheme is much less that the discontinuity associated with the switch from the staircasing scheme.

However, even when staircasing is used to handle cells that have small areas outside of the PEC, the behavior illustrated in Figs. (4)–(6) is not a significant disadvantage of the D-FDTD method since, in practice, one always tries to use the coarsest possible discretization. Moreover, the amount of phase error associated with a grid distortion of 1/15th of a cell when using 27 points per wavelength is quite small (i.e., when the D-FDTD and CP-FDTD methods have nearly equal accuracy, the unnormalized error is already small).

Finally, Fig. 7 shows the error as a function of incident angle when the PEC plane has a fixed offset of 0.2 and N_λ is eight. Since the phase change for movement in the x-direction goes to zero as the incident angle θ approaches 90°, the phase error also goes to zero. Note that the D-FDTD method provides the superior result.

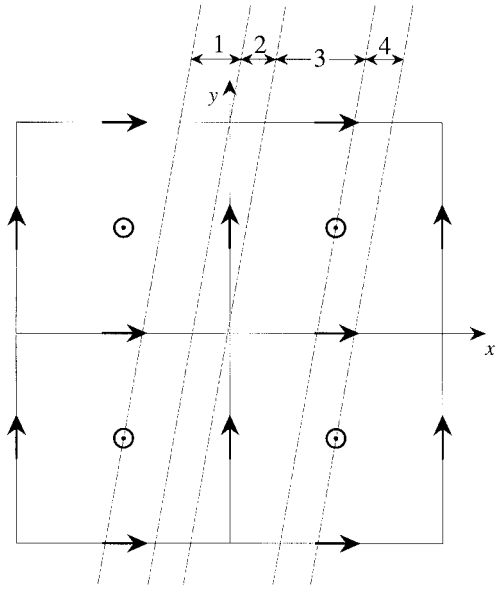

Fig. 8. Section of the FDTD grid showing different ranges of position for the PEC boundary.

III. Comparison of Algorithms for a Sloping PEC Surface

Consider the situation in which the FDTD mesh is intersected by a free-space/PEC boundary, as shown in Fig. 8. In this example, the boundary is at an angle of 10° to the y-axis and may intercept the x-axis at any point. The dashed lines demarcate four ranges of PEC positions, each one of which may require different treatment by the modified FDTD algorithms considered. The circles represent the H_z nodes and the arrows represent the E nodes. The cell sizes are assumed to be δx and δy and the intercepts of the PEC boundary with the lines $y = \delta y$ and $y = 0$ are given by b_1 and b_2, respectively. The pertinent properties of the different ranges can be summarized as follows.

Range 1: The H_z node at $(-\delta x/2, \delta y/2)$ is outside the PEC, but the cell centered at $(\delta x/2, \delta y/2)$ is totally inside the PEC, and both neighboring E_x nodes are available.

Range 2: The area of the cell centered at $(\delta x/2, \delta y/2)$, which is outside the PEC, is greater than zero, but either this area is less than a specified percentage of the total or the ratio of the maximum contour length outside the PEC to the cell area outside the PEC is greater than a specified value.

Range 3: The area of the cell centered at $(\delta x/2, \delta y/2)$, which is outside the PEC, is greater than the specified percentage of the total and the ratio of maximum contour length to the cell area is less than its specified value, but the H_z node at $(\delta x/2, \delta y/2)$ is inside the PEC.

Range 4: The H_z node at $(\delta x/2, \delta y/2)$ is outside the PEC, but one or both of the E_x nodes at $(\delta x/2, 0)$ and $(\delta x/2, \delta y)$ are unavailable either because they are inside the PEC or because the H nodes needed to update them using the standard FDTD algorithm are inside the PEC.

Under these circumstances, the algorithms being considered will treat the update of $H_z(-\delta x/2, \delta y/2)$ in the following ways.

Range 1: The H_z node at $(-\delta x/2, \delta y/2)$ is, in all the algorithms, updated using the following equation for the contracted cell:

$$\frac{\delta_t H_z\left(-\frac{\delta x}{2}, \frac{\delta y}{2}\right)}{\delta t} = \frac{1}{A_1 + A_2} \cdot \left\{ \delta y E_y\left(-\delta x, \frac{\delta y}{2}\right) + (\delta x + b_1) E_x\left(-\frac{\delta x}{2}, \delta y\right) - (\delta x + b_2) E_x\left(-\frac{\delta x}{2}, 0\right) \right\} \tag{32}$$

where δ_t is used to indicate the central difference operator and A_1 and A_2 correspond to the areas of the cells centered at $(-\delta x/2, \delta y/2)$ and $(\delta x/2, \delta y/2)$, respectively, that are outside of the PEC. Area A_2 will be zero throughout Range 1, but this equation is also applied, as noted below, when this term is not zero.

Range 2: When there is a very small area of a cell, which is outside the PEC, the D-FDTD method, as used here, treats the whole cell as being inside the PEC. (As noted previously, an alternative approach is to employ the CP-FDTD scheme in these cases.) Thus, all the algorithms use (32), except the D-FDTD technique which uses

$$\frac{\delta_t H_z\left(-\frac{\delta x}{2}, \frac{\delta y}{2}\right)}{\delta t} = \frac{1}{A_1} \left\{ \delta y E_y\left(-\delta x, \frac{\delta y}{2}\right) + \delta x E_x\left(-\frac{\delta x}{2}, \delta y\right) - \delta x E_x\left(-\frac{\delta x}{2}, 0\right) \right\}. \tag{33}$$

Range 3: For the D-FDTD method, $H_z(\delta x/2, \delta y/2)$ is updated, notwithstanding the fact that it is inside the PEC, using the following equation:

$$\frac{\delta_t H_z\left(\frac{\delta x}{2}, \frac{\delta y}{2}\right)}{\delta t} = \frac{1}{A_2} \left\{ \ell_y E_y\left(0, \frac{\delta y}{2}\right) + b_1 E_x\left(\frac{\delta x}{2}, \delta y\right) - b_2 E_x\left(\frac{\delta x}{2}, 0\right) \right\} \tag{34}$$

where ℓ_y is the length of the contour associated with the node $E_y(0, \delta y/2)$ that is outside of the PEC. If ℓ_y is less than δy, the coefficient of $E_x(\delta x/2, 0)$ is set to zero (i.e., if the x intercept is less than zero, $E_x(\delta x/2, 0)$ is unused). Using this result, all the E field nodes are updated using the standard FDTD equations, thence $H_z(-\delta x/2, \delta y/2)$ is updated.

For the other three algorithms, the cell is expanded and $H_z(-\delta x/2, \delta y/2)$ is updated directly using (32). Since no borrowing has taken place, all of these algorithms use the same update equation.

Range 4: Here, the node $H_z(\delta x/2, \delta y/2)$ is outside the metal and is updated in all the algorithms. However, because the node at $E_x(\delta x/2, 0)$ cannot be updated using the standard FDTD algorithm, this value is "borrowed" from its nearest neighbor, viz. $E_x(-\delta x/2, 0)$. The update equation for $H_z(\delta x/2, \delta y/2)$ is given by

$$\frac{\delta_t H_z\left(\frac{\delta x}{2}, \frac{\delta y}{2}\right)}{\delta t} = \frac{1}{A_2} \left\{ \delta y E_y\left(0, \frac{\delta y}{2}\right) + b_1 E_x\left(\frac{\delta x}{2}, \delta y\right) - K b_2 E_x\left(-\frac{\delta x}{2}, 0\right). \right\} \tag{35}$$

In the CP-FDTD and the stabilized CP-FDTD algorithms, K takes the value of unity, in the A-FDTD algorithm, it can be given a value between zero and unity, but must be set to zero if late time stability is to be guaranteed.

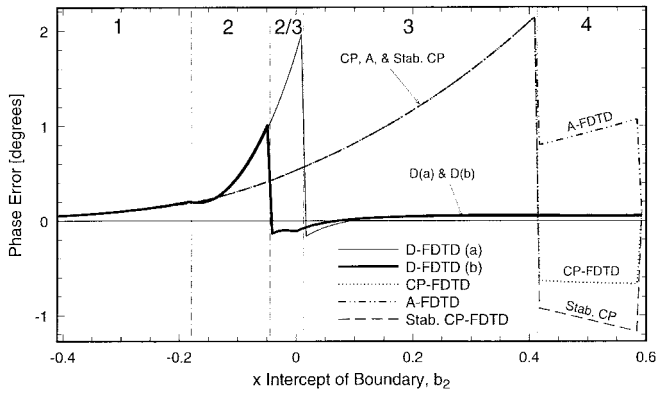

Fig. 9. Error in the total field predicted by the different algorithms.

In the CP-FDTD and A-FDTD methods, the E_x node at $(-\delta x/2, 0)$ is updated using the standard FDTD equations, but the stabilized CP-FDTD algorithm uses a modified update equation in order to restore reciprocity as follows:

$$\frac{\delta_t E_x\left(-\frac{\delta x}{2}, 0\right)}{\delta t} = \frac{1}{\delta y} \cdot \left\{ \frac{\delta x}{\delta x + b_2} H_z\left(-\frac{\delta x}{2}, \frac{\delta y}{2}\right) + \frac{b_2}{\delta x + b_2} H_z\left(\frac{\delta x}{2}, \frac{\delta y}{2}\right) + -H_z\left(-\frac{\delta x}{2}, -\frac{\delta y}{2}\right) \right\}. \quad (36)$$

IV. Errors in Predicted Total Field

To demonstrate the effect of these different ways of treating the update equations, the following test was performed. The geometry of Fig. 8 was used with the PEC boundary set at an angle of 10° to the y-axis and parallel to the z-axis. Excitation takes the form of an incident plane wave, which propagates in the x-direction and is polarized with E in the y-direction. The cell size was set at $\lambda/10$ and the Courant number was $0.95/\sqrt{3}$ for all algorithms, except the D-FDTD method, for which a time step shown to give stable results was used [13], [14]. In order to isolate as much as possible the errors due to the discretization method from those caused by dispersion in the underlying unmodified mesh, the speed of propagation was assumed to be that in the unmodified FDTD mesh as given by (12), not the free-space value. Assuming exact field values in the mesh at all times before $(t - \delta t)$, the error in the predicted value of $H_z(-\delta x/2, \delta y/2)$ at time t from each algorithm was calculated. The results are shown in Fig. 9 where the phase error is plotted versus the x intercept b_2 of the PEC boundary.

The ranges of positions for the PEC boundary as a function of the x intercept are as follows where the $*$ indicates a typical value, which will depend on the parameters chosen for the D-FDTD algorithm.

Range 1: $-0.41\delta x < b_2 < -0.18\delta x$;
Range 2: $-0.18\delta x < b_2 < -0.01\delta x*$;
Range 3: $-0.01\delta x* < b_2 < 0.41\delta x$;
Range 4: $0.41\delta x < b_2 < 0.59\delta x$.

Results are given for the D-FDTD method under two different conditions corresponding to the limiting conditions on the shape and size of a cell given in [13] and [14]. The curves are as follows: cell area greater than 2.5%, ratio of contour length to area less than 10, stability factor $0.7/\sqrt{3}$ and cell area greater than 1.5%, ratio of contour length to area less than 15, stability factor $0.5/\sqrt{3}$. The time steps used for curves (a) and (b) are those given in [13] and [14], which were found to yield stable results. The main effect of these different conditions is in the position of the boundary between Ranges 2 and 3. The range of positions labeled as "2/3" in Fig. 9 will be in Ranges 2 or 3 depending on the choice of conditions for the D-FDTD method. None of the other algorithms are affected by this.

From Fig. 9, it can be seen that all the algorithms give the same error when the PEC boundary is in Range 1, as would be expected. For Ranges 2 and 3, the error given by all algorithms, except the D-FDTD method, show a steady increase with b_2. This can be explained by the fact that the cell size is increasing, therefore, the discretization error will also increase. In addition, the position of the H node, which is being updated, remains at its assigned place and is, therefore, no longer at the barycenter of the cell. In contrast to this, the error produced by the D-FDTD method remains at a low level with the exception of Range 2 and the region near it in Range 3.

Although, as with the other methods, errors will be caused by the changing cell size and the positioning of the H node at some distance from the center of the cell, this error is mitigated because the cell is always contracted, not expanded. Moreover, the greatest error from the nonoptimum placement of the H node occurs when the cell is at its smallest, and since the H field is tangential to the PEC boundary and has a very low normal derivative, the overall effect is small. This is the opposite of the situation when expanded cells are used.

In Range 4, nearest neighbor borrowing is required in all but the D-FDTD method and each of the algorithms gives a different result depending on the details of how the borrowing is done. As before, the error in the D-FDTD algorithm, which needs no special treatment in this case, remains at a low level. Of the other methods, the CP-FDTD method gives the next lowest error of approximately 1°, but is not guaranteed to be stable. The A-FDTD algorithm overcomes the stability problem by setting the borrowed field to zero, whereas the stabilized CP-FDTD algorithm increases the size of the finite-difference stencil in order to restore reciprocity. The errors for the latter two methods are, for this particular example, similar in magnitude, but opposite in sign.

V. Numerical Results

In order to compare the performance of the different algorithms on typical 3-D structures, a variety of scattering and resonant cavity problems were addressed, including spheres, cylinders placed at an angle to the Cartesian mesh, and cones. The overall trend was similar in every case, thus, for brevity, just two different cases are presented here. The first is that of a resonant spherical cavity, which is the only completely 3-D

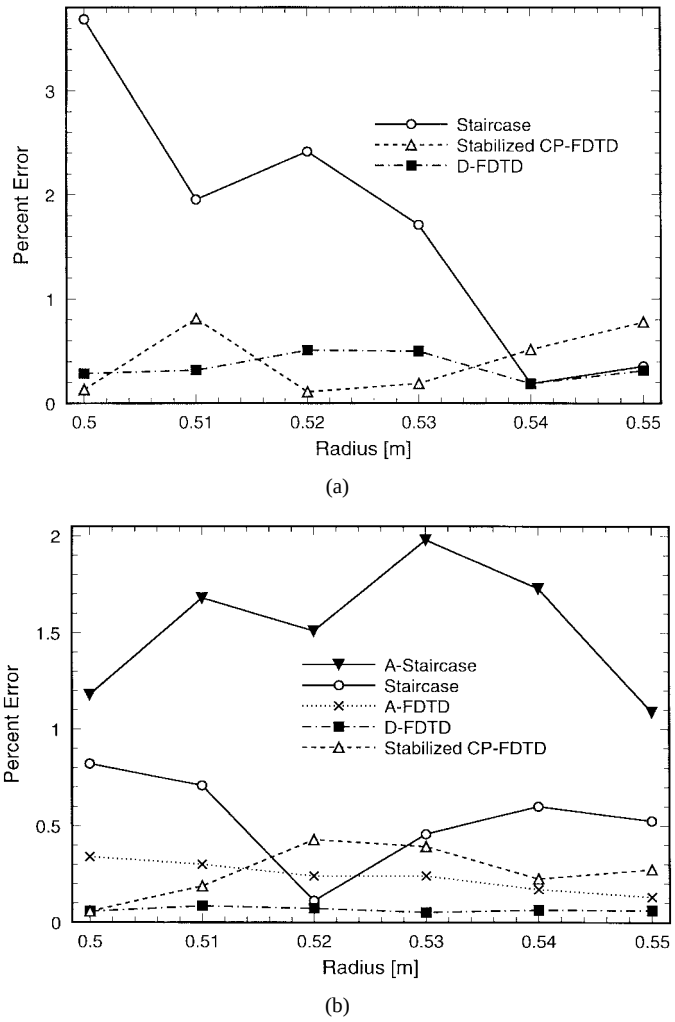

Fig. 10. Percent error in the resonant frequency of the dominant mode of a spherical cavity versus radius. (a) Coarse grid with grid spacing 0.10 m. (b) Fine grid with grid spacing 0.05 m.

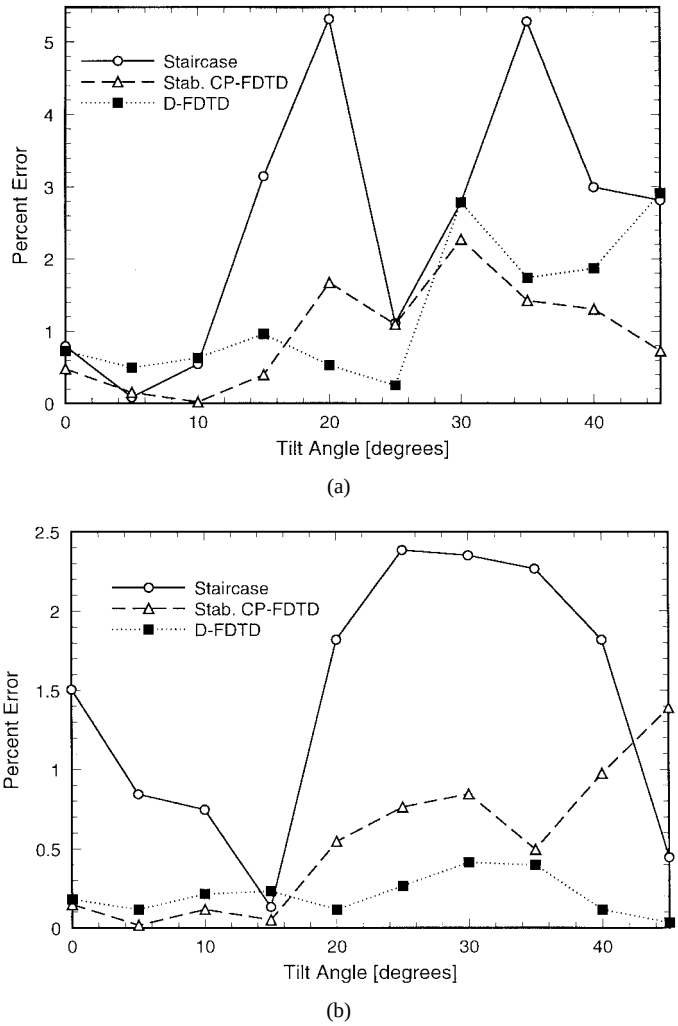

Fig. 11. Percent error in the resonant frequency of the dominant mode of a cylindrical cavity versus tilt angle. The cavity has a height of 0.30 m and a radius of 0.19 m. (a) Coarse grid with grid spacing 0.050 m. (b) Fine grid with grid spacing 0.025 m.

structure for which results were presented in [10]. The second is a circular cylindrical cavity, which is tilted with respect to the axes.

A. Spherical Resonant Cavity

In Fig. 10, the errors in the calculated resonant frequencies of a spherical cavity are plotted as a function of radius for each of the different curved-surface algorithms and for two different cell sizes. The results for the coarse mesh, which has approximately five cells per radius or roughly 12 cells per wavelength at the resonant frequency, the results from the stabilized CP-FDTD scheme, and the D-FDTD scheme are very similar and, with a few exceptions, are better than the staircase approximations. The exceptions where the staircase actually performs better than the curved-surface algorithms can be explained by the fact that the staircasing error is a complex function of the test geometry and its placement within the mesh. This function may, in isolated cases, take a small or even zero value. Nevertheless, the more advanced algorithms will reliably provide a lower *average* error. The unstabilized CP-FDTD method indeed exhibited late time instability irrespective of the chosen time step and no results could be obtained for this structure.

The results for the fine mesh, approximately ten cells per radius or 24 cells per wavelength at the resonant frequency, include the results presented in [10], as well as from the stabilized CP-FDTD and D-FDTD methods. Again, no results could be obtained using the unstabilized CP-FDTD. Here it can be seen that the D-FDTD scheme substantially outperforms the other methods and, moreover, is the most consistent over the range of radii considered. The results from the A-FDTD method, taken from [10] and the stabilized CP-FDTD, are similar on average. This would be expected from the results presented in Section IV. Two different results are given for the staircase approximation. The line with the open circles shows results calculated by the authors in which each *square* was assigned to the PEC if its center was in the PEC. The line with filled triangles, labeled A-Staircase, corresponds to results taken from [10] in which, it is assumed, each *cube* was assigned to PEC if its center was in the PEC. Clearly, the former method of staircasing gives a better result which

actually outperforms the CP-FDTD and A-FDTD algorithms at radii in the vicinity of 0.52 m.

B. Cylindrical Resonant Cavity

As an example which includes the effects of sharp corners as well as sloping and curved boundaries, a cylinder of radius 0.19 m and height 0.3 m, which is tilted with respect to the Cartesian axes, is analyzed. In Fig. 11, the error in the calculated resonant frequency of the dominant mode of this structure is plotted as a function of the angle of tilt for the staircase approximation, the stabilized CP-FDTD method, and the D-FDTD method. The results are calculated using two different cell sizes, these being 0.05 m, or approximately four cells per radius (ten cells per wavelength at the resonant frequency), and 0.025, which is approximately eight cells per radius (20 cells per wavelength at the resonant frequency).

It can be seen that, for the coarse mesh, the D-FDTD method and the stabilized CP-FDTD method give similar errors, both of which are, on average, much less than the staircase method. For the fine mesh, the D-FDTD method gives the lowest average error, while both the D-FDTD and stabilized CP-FDTD methods show a considerable improvement over the staircase method, with the exception of angles of tilt in the vicinity of 15°.

VI. Conclusion

In this paper, some of the algorithms for the treatment of curved PEC boundaries have been investigated both analytically and numerically. It has been shown that, despite its simplicity, the D-FDTD method is typically more accurate than the alternatives. The reasons for this can be summarized as follows. Firstly, although all the algorithms correctly represent the position of the boundary, in the D-FDTD method the distorted cells are contracted, never expanded. Thus, the discretization error caused by the numerical approximation to the spatial derivatives will always be reduced, rather than increased. Secondly, in all the algorithms, the position of the H node remains at its assigned place even though the contour which surrounds it is distorted. Since this means that the H node is not at the barycenter of the distorted cell, an extra error will be introduced. For an expanded cell, the magnitude of this error will be largest when the expanded cell is largest, whereas for the contracted cell, this error will be largest when the cell is smallest. It is observed that in the latter case, the PEC is very close to the edge of the cell and, thus, the spatial derivative of the H field in the contracted cell is likely to be small. Therefore, in this case, the error in placement of the H node will have little effect on the overall result. On the other hand, for the case of the expanded cell, the spatial derivative of the H field will be larger and, therefore, the overall effect of an error in the placement of the H node will be greater. The only penalty of using the D-FDTD method is a necessary reduction in time step, but this is considered a small price in view of the much greater saving of resources which result from using the method.

Acknowledgment

The first author, C. J. Railton, wishes to thank Prof. J. McGeehan for the provision of facilities within the Centre for Communications Research.

References

[1] A. C. Cangellaris and D. B. Wright, "Analysis of the numerical error caused by the stair-stepped approximation of a conducting boundary in FDTD simulations of electromagnetic phenomena," *IEEE Trans. Antennas Propagat.*, vol. 39, pp. 1518–1525, Oct. 1991.

[2] R. Holland, "Pitfalls of staircase meshing," *IEEE Trans. Electromag. Compat.*, vol. 35, pp. 434–439, Nov. 1993.

[3] J. B. Schneider and K. L. Shlager, "FDTD simulations of TEM horns and the implications for staircased representations," *IEEE Trans. Antennas Propagat.*, vol. 45, pp. 1830–1838, Dec. 1997.

[4] T. G. Jurgens, A. Taflove, K. Umashankar, and T. G. Moore, "Finite-difference time-domain modeling of curved surfaces," *IEEE Trans. Antennas Propagat.*, vol. 40, pp. 357–366, Apr. 1992.

[5] T. G. Jurgens and A. Taflove, "Three-dimensional contour FDTD modeling of scattering from single and multiple bodies," *IEEE Trans. Antennas Propagat.*, vol. 41, pp. 1703–1708, Dec. 1993.

[6] N. K. Madsen, "Divergence preserving discrete surface integral methods for Maxwell's curl equations using nonorthogonal unstructured grids," Lawrence Livermore Nat. Lab., Tech. Rep. UCRL-JC-109787, Feb. 1992.

[7] ———, "Divergence preserving discrete surface integral methods for Maxwell's curl equations using non-orthogonal unstructured grids,"*J. Comput. Phys.*, vol. 119, pp. 34–45, 1995.

[8] I. J. Craddock, C. J. Railton, and J. P. McGeehan, "Derivation and application of a passive equivalent circuit for the finite difference time domain algorithm," *IEEE Microwave Guided Wave Lett.*, vol. 6, pp. 40–42, Jan. 1996.

[9] M. Okoniewski, J. Anderson, M. Mrozowski, and S. S. Stuchly, "Arbitrarily located metal surfaces in FDTD technique," in *Progress in Electromag. Res. Symp.*, Seattle, WA, July 1995, p. 178.

[10] J. Anderson, M. Okoniewski, and S. S. Stuchly, "Practical 3-D contour/staircase treatment of metals in FDTD," *IEEE Microwave Guided Wave Lett.*, vol. 6, pp. 146–148, Mar. 1996.

[11] C. J. Railton and I. J. Craddock, "Analysis of general 3-D PEC structures using improved CP-FDTD algorithm," *Electron. Lett.*, vol. 31, pp. 1553–1554, Sept. 1995.

[12] ———, "Stabilised CP-FDTD algorithm for the analysis of arbitrary 3D PEC structures," *Proc. Inst. Elect. Eng.*, vol. 143, pt. H, pp. 367–372, Oct. 1996.

[13] S. Dey, R. Mittra, and S. Chebolu, "A technique for implementing the FDTD algorithm on a nonorthogonal grid," *Microwave Opt. Technol. Lett.*, vol. 14, pp. 213–215, Mar. 1997.

[14] S. Dey and R. Mittra, "A locally conformal finite-difference time-domain (FDTD) algorithm for modeling three-dimensional perfectly conducting objects," *IEEE Microwave Guided Wave Lett.*, vol. 7, pp. 273–275, Sept. 1997.

[15] S. G. García, T. M. Hung-Bao, B. G. Olmedo, and R. G. Martín, "Volume-conformation method to study scattering by PEC objects with FDTD," *Proc. Inst. Elect. Eng.* vol. 143, pt. H, pp. 131–136, Apr. 1996.

[16] M. Celuch-Marcysiak and W. K. Gwarek, "Higher order modeling of media interfaces for enhanced FDTD analysis of microwave circuits," in *24th European Microwave Conf.*, Cannes, France, Sept. 1994, pp. 1530–1535.

[17] Y. Hao and C. J. Railton, "Analyzing electromagnetic structures with curved boundaries on Cartesian FDTD meshes," *IEEE Trans. Microwave Theory Tech.*, vol. 46, pp. 82–88, Jan. 1998.

[18] W. K. Gwarek, "Analysis of an arbitrarily-shaped planar circuit—A time-domain approach," *IEEE Trans. Microwave Theory Tech.*, vol. MTT-33, pp. 1067–1072, Oct. 1985.

[19] M. Celuch-Marcysiak and W. Gwarek, "Generalized TLM algorithms with controlled stability margin and their equivalence with finite-difference formulations for modified grids," *IEEE Trans. Microwave Theory Tech.*, vol. 43, pp. 2081–2089, Sept. 1995.

[20] A. Taflove, *Computational Electrodynamics: The Finite-Difference Time-Domain Method*. Norwood, MA: Artech House, 1995.

[21] ———, "Review of the formulation and applications of the finite-difference time-domain method for numerical modeling of electromagnetic wave interactions with arbitrary structures," *Wave Motion*, vol. 10, no. 6, pp. 547–582, 1988.

Chris J. Railton (M'88) received the B.Sc. degree in physics with electronics from the University of London, London, U.K., in 1974, and the Ph.D. degree in electronic engineering from the University of Bath, Bath, U.K., in 1988.

From 1974 to 1984, he worked in the scientific civil service on a number or research and development projects in the areas of communications, signal processing, and electromagnetic compatibility (EMC). From 1984 to 1987, he was with the University of Bath, where he was involved in the mathematical modeling of boxed microstrip circuits. He is currently with the Centre for Communications Research, University of Bristol, Bristol, U.K., where he leads the Computational Electromagnetics Group, which is engaged in the development of new algorithms for electromagnetic analysis and their application to the design of monolithic microwave integrated circuits (MMIC's), planar and conformal antennas, microwave and RF heating systems, EMC, high-speed interconnects, and optical waveguide components.

John B. Schneider (M'92) received the B.S. degree in electrical engineering (*summa cum laude*) from Tulane University, New Orleans, LA, and the M.S. and Ph.D. degrees in electrical engineering from the University of Washington, Pullman.

He is currently an Associate Professor in the School of Electrical Engineering and Computer Science, Washington State University. His research interests include the use of computational methods to analyze acoustic, elastic, and electromagnetic wave propagation.

Dr. Schneider received an Office of Naval Research Young Investigator Award in 1996.